ChemPubSoc Europe

DOI: 10.1002/chem.201604923

CHEMISTRY
A European Journal
Communication

Piezochromic Effects

Enhanced Sensitivity and Piezochromic Contrast through Single-Direction Extension of Molecular Structure

Zhao Gao,[a] Kai Wang,[b] Fangming Liu,[a] Cunfang Feng,[a] Xin He,[a] Jinyu Li,[a] Bing Yang,[a] Bo Zou,*[b] and Ping Lu*[a]

Abstract: Two piezochromic materials containing phenanthro[9,10-*d*]imidazole and tetraphenylethylene (M1 and M2) were developed. A supra-amplification piezochromic effect originating from their various long-to-short axis ratios was discovered in high-pressure experiments. Based on the linear relationship between applied pressure and emission-peak wavelength during pressurizing and depressurizing cycles, quantitative sensitivity for piezochromism could be denoted. M2 displayed higher piezochromic contrast (102 nm) and better sensitivity (11.19 nm GPa^{-1}) than M1 (69 nm and 6.12 nm GPa^{-1}), which helps to develop a more comprehensive general strategy to evaluate pressure-responsive performance.

Smart materials have attracted tremendous attentions in recent years, driven by the human demand for accurate responses to external changes in real time.[1] Pressure is one of the most common natural stimuli. Those materials that enable the translation of the physical impact from pressure into a change of emission property are usually defined as piezochromic materials.[1c,2] The challenge for precise and gradient pressure measurements in various environments such as marine research, underground geochemistry, wind tunnels, and aircraft industries,[3,4] promotes the pursuit for piezochromic materials sensitive to high external pressure and giving observable signals.[5] Since the discovery of the difference between anisotropic grinding and isotropic compression with tetrathiazolylthiophene as the model compound, which displayed reversible luminescent chromism at an applying pressure of 3.2 GPa,[6] a rapid expansion has been sparked in the field of piezochromic materials responsive to high external pressure.[7,8] A number of small organic molecules,[9] metal complexes,[10] and polymers[1c,11] have been tested. Recently, visible-light alteration of the organolead–bromide perovskite under hydrostatic pressure up to 34 GPa was reported.[12] These inspiring results demonstrated the great potential of the materials for their application as pressure sensors. However, there are still important unresolved fundamental problems that hamper further applications. Most piezochromic materials are discovered serendipitously, and these reports[5–12] are relatively independent. It is difficult to estimate the sensitivity of various kinds of compounds. Very limited systematic investigations have been performed concerning the question of how to manipulate the ability of responding to high external pressure, as well as how to influence piezochromic color contrast and reversibility by adjusting the molecular structure. With these considerations in mind, in this work, we focused on regulating the piezochromic property through molecular design for a general strategy to further promote the development of piezochromic materials.

In general, the luminescence quantum yield of organic compounds decreases with increasing external pressure.[1b,13] A preliminary requirement to access excellent piezochromic materials is that the organic dye should exhibit high quantum efficiency. In prior studies, materials with aggregation induced emission (AIE) characteristics were important resources for piezochromic materials.[14,15] Tetraphenylethylene (TPE) is a typical AIE luminogen that processes a simple molecular structure.[16–19] However, TPE is non-piezochromic, which is believed to result from the quick recrystallization driven by multiple intermolecular interactions and rigid near-spherical geometry that can consume the external stress by free sliding or rolling.[20] To endow it with piezochromic property, one promising way is coupling with an appropriate group that can emit high fluorescence in the solid state asymmetrically to disrupt the near-spherical geometry of TPE. Phenanthro[9,10-*d*]imidazole (PI) was proven to be a class of dye with high solid-state quantum yield and good thermal stability in our previous work.[21–24] Here, the two materials M1 and M2 were designed by attaching a PI unit to one of the phenyl rings of TPE to obtain an extended molecular structure. The distance between twisted TPE and planar PI is determined by the center-linked benzene ring. In this approach, the long-to-short axis ratios of M1 and M2 were tuned accordingly. In addition, combing the two units may generate an interesting molecular stacking structure. The propeller structure of TPE could lead to a relatively loose packing mode that would resist high external pressure without collapse.[2b,19b] PI, with rigid molecular structure, might reduce the non-radiative transitions and enhance the change of fluorescent signal. In the high-pressure experiment, it was found that the emission-peak wavelengths of M1 and M2 had a one-di-

[a] Dr. Z. Gao, Dr. F. Liu, Dr. C. Feng, Dr. X. He, Dr. J. Li, Prof. B. Yang, Prof. P. Lu
State Key Laboratory of Supramolecular Structure and Materials
Jilin University, Qianjin Street No. 2699, Changchun 130012 (P. R. China)
E-mail: lup@jlu.edu.cn

[b] Dr. K. Wang, Prof. B. Zou
State Key Laboratory of Superhard Materials
Jilin University, Qianjin Street No. 2699, Changchun 130012 (P. R. China)
E-mail: zoubo@jlu.edu.cn

Supporting Information for this article can be found under http://dx.doi.org/10.1002/chem.201604923.

mensional linear relationship with the applied pressure, which was varied from 0.0 to 10.1 GPa, accompanied by visible colorimetric changes with good reversibility. M2 exhibited a better piezochromic contrast with a much bigger wavelength redshift than M1 (102 and 69 nm, respectively). The sensitivity was denoted according to the slope of the curve (emission wavelengths vs. pressure), which demonstrated that M2 shows a twofold higher sensitivity than M1, caused by the extension of the long-to-short axis ratio by one extra phenyl ring in the center of the molecule for M2.

M1 and M2 were synthesized with good yields by Suzuki coupling reactions (Scheme S1).[22a,25] The final products were characterized by NMR spectroscopy, high-resolution MS, FTIR, and elemental analysis, and corresponded well to their expected structures (see Supporting Information). The thermogravimetric analysis (TGA) revealed that the decomposition temperature (5% weight loss) was 378 °C for M1 and 456 °C for M2, demonstrating their good thermal stability (Figure S3a in the Supporting Information).

To understand the molecular structure and packing in the solid state, a single-crystal X-ray diffraction (XRD) study was performed. Fortunately, the crystal of M1 was obtained successfully by slow diffusion of petroleum into a chloroform solution. As shown in Figure 1, the crystalline lattice of M1 indicates that TPE adopts a twisted conformation and PI retains a planar conformation, with a relatively big dihedral angel of 57° between the TPE and PI planes. An antiparallel arrangement is observed, that is, the TPE and PI units are stacked alternately based on a head-to-tail arrangement. The intermolecular interactions between PI units are thus interrupted effectively. As a result, the formation of excimers or exciplexes through π–π stacking, commonly observed for planar molecules, is prevented in the crystal,[18b] leading to its high quantum efficiency. Multiple C–H···π hydrogen bonds are formed between the hydrogen atoms of the TPE phenyl rings and the π-electrons of PI (Figure 1b). The interplane distance between adjacent TPE and PI units is 2.778–3.066 Å. These multiple C–H···π hydrogen bonds could help to rigidify the molecular conformation and lock the molecular rotations of TPE, which reduces the energy loss through the non-radiative rotational relaxation channel and thus further enhances the emission efficiency. All these features enable M1 to show intense solid-state emission. The quantum efficiency of the M1 crystal was as high as 85%. In addition, the powders of M1 and M2 also exhibited strong blue emission peaking at 468 and 462 nm, respectively, with high quantum efficiencies of nearly 90%.

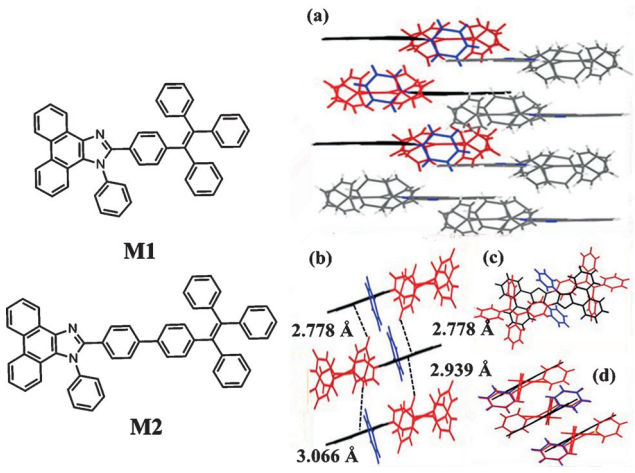

Figure 1. Molecular structures of M1 and M2, and the molecular packing of M1: a) Side view; b) C–H···π hydrogen-bond interactions; c) top view; (d) front view.

M1 and M2 were sensitive to mechanical grinding and showed completely reversible fluorescence-emission changes. M1 displayed a redshift from 468 to 486 nm (18 nm) after grinding with a 17 nm increase of full width half maximum (FWHM), whereas M2 showed a redshift from 462 to 472 nm (10 nm) with an enhanced FWHM of 35 nm (Figure S7 in the Supporting Information). The wide-angle XRD (WXRD) indicated that the ground samples of M1 and M2 were amorphous phases (Figure S9 in the Supporting Information), whereas the original ones showed remarkable crystalline features at $2\theta < 25°$. The differential scanning calorimetry (DSC) curves (Figure S3 in the Supporting Information) of M1 and M2 in different solid states confirmed that the two samples show different metastable aggregation structures. These phenomena are in accordance with the mechanistic explanations reported in other systems.[9b] However, based on the alternations of redshifts and FWHMs of M1 and M2, it is difficult to comment on the superiority between these two compounds because of a lack of conventional evaluation standards for piezochromism.

A significantly enhanced piezochromic contrast was observed under high external pressure. The high-pressure experiments were performed by placing the samples in the holes of a T301 steel gasket with silicone oil as a pressure-transmitting medium. If the applied pressure was gradually increased from 0.0 to 10.1 GPa, the emission peak of M2 depicted a large-scale redshift from 462 (blue emission) to 564 nm (orange emission) (Figure 2a). At the same time, the luminescence intensity of M2 was reduced continuously. The emission intensity at 10.1 GPa remained only 1/64 of that at 0.0 GPa. If the external pressure was fully released, the emission-peak wavelength and intensity of M2 were completely restored to its original state, indicating its good reversibility (Figure 2b). The emissions could be switched between 462 and 564 nm (102 nm redshift) during pressurizing–depressurizing cycles many times without any fatigue (Figure 2c), further confirming a good reversibility. For M1, the reversible emission switch between 468 and 537 nm (69 nm redshift) could be repeated by pressurizing–depressurizing cycles from 0.0 to 10.1 GPa (Figure S12 in the Supporting Information). The emission-peak wavelength showed a linear relationship with the applied pressure in both pressurizing and depressurizing cycles of M1 and M2 (Figure 2d). This implies that, as long as the emission wavelength of the material is measured, the value of the external pressure can be determined very conveniently. The results provide the possibility to compare the sensitivity quantitatively. The slope of the wavelength–pressure curve was calculated by the following equation [Eq. (1)]:

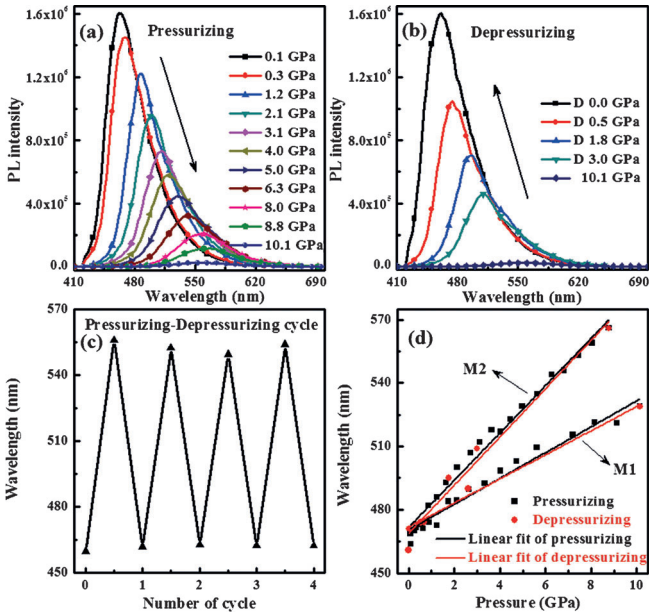

Figure 2. Fluorescence spectroscopy of M2 at various pressures from 0.0 to 10.1 GPa: a) Pressurizing; b) depressurizing; c) reversible switch of emission of M2 by pressurizing–depressurizing cycle; d) pressure versus emission-peak wavelength during the pressurizing–depressurizing cycle. A UV-LED lamp was used for the excitation (λ_{ex} = 405 nm).

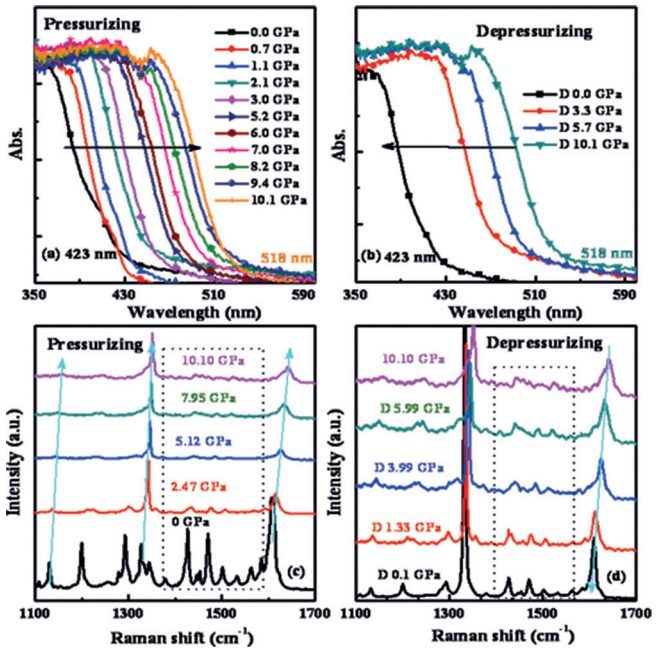

Figure 3. In situ UV/Vis absorption and Raman spectroscopy in the range of 1100–1700 cm^{-1} of M2 at various pressures from 0.0 to 10.1 GPa: a), c) Pressurizing and b), d) depressurizing.

$$k = \frac{\lambda_1 - \lambda_2}{P_1 - P_2} \quad (1)$$

in which k represents the slope of the curves, and λ_1 and λ_2 refer to the maximum emission-peak wavelengths at pressures of P_1 and P_2, respectively. Thus, the k value of M2 was calculated to be 11.19 nm GPa^{-1} according to the linear fit in the pressurizing cycle. In comparison, the k value of M1 was 6.12 nm GPa^{-1}. The approximately twofold higher k value of M2 illustrates its better sensitivity. Unlike the similar piezochromic property of M1 and M2 at ambient conditions, there exists a supra-amplification effect originating from the increased long-to-short axis ratio in high-pressure experiments, demonstrating the superiority of M2.

During the compression, better planarity of TPE and closer molecular packing may be induced by pressure, which would manifest in the formation of excimer. This effect is more severe in M2 owing to the longer effective conjugation length that increases the overlap of π-electrons and gives rise to a larger redshift. To understand the physics behind the effect, high-pressure in situ UV/Vis absorption spectra of M1 and M2 up to 10.1 GPa were measured. As shown in Figure 3a, the absorption sidebands were gradually shifted to longer wavelengths and broadened continuously, indicating that the energy gaps were gradually reduced with increasing pressures. For M2, the optical energy gap was calculated to be approximately 2.93 eV from the sideband of UV absorption at 423 nm at ambient pressure, which belongs to the category of blue-emission material. At 10.1 GPa, this sideband was shifted to 518 nm, and the optical energy gap was changed to 2.39 eV. M1 displayed a similar alteration of the energy gap with a change from 2.76 to 2.04 eV. Notably, by releasing the applied pressure, the UV spectrum was restored to the initial one, which is consistent with the results of high-pressure fluorescence spectroscopy. The reduced energy gap can be attributed to the flattening of molecular rings in the TPE unit because PI readily adopts a planar conformation. Further proof was obtained by using in situ Raman spectroscopy. The Raman spectra in the range of 1100–1700 cm^{-1} at different pressures were applied to track the changing molecular structure. The Raman peak at 1133 cm^{-1} was attributed to the stretching vibration of the C–C bond formed between ethylene and the benzene ring in TPE. The peak at approximately 1600 cm^{-1} resulted from the stretching vibrations of C=C and the benzene ring.[26] As shown in Figure 3c, the peak from the stretching vibration displays a significant blueshift from 1606 to 1640 cm^{-1} with increasing pressure, indicating that the bond lengths are shortened. In addition, all the Raman peak intensities gradually weakened, illustrating that molecular vibrations are limited by the close packing induced by pressure, which causes a loss of Raman vibration activity and intensity. The shortened intermolecular distance could enhance the polarization effect of adjacent molecules, which would reduce the energy of the lowest excited state and the radiative transition rate, leading to a redshift in the fluorescent wavelength and a decrease in photoluminescence (PL) intensity.[27] The effect was intensified in M2 owing to the more conjugated structure, which generates higher piezochromic contrast in emission wavelength. If the hydrostatic pressure returned to atmospheric level, all Raman peaks were recovered, which indicates that the changes in molecular conformation are completely reversible. There was no peak degeneration or splitting in the in situ absorption and Raman spectra, meaning that no phase transition occurred during the pressurization. Thus, the spectra change originates

from the change of molecular conformation and enhanced intermolecular interactions.

The in situ angle-dispersive XRD (ADXRD) pattern with high-intensity synchrotron radiation further offered an opportunity to track the pressure influence during compression and release (Figure 4). All the diffraction peaks of M2 shifted to higher

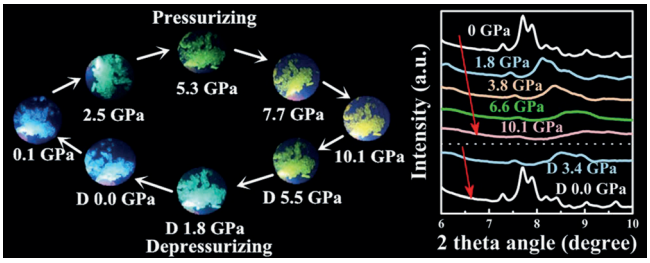

Figure 4. a) Micrographs of M2 at pressures from 0 to 10.1 GPa. A UV-LED lamp was used for the excitation ($\lambda_{ex}=405$ nm); b) in situ ADXRD patterns of the M2 crystal at various pressures.

angles from 0 to 3.8 GPa, demonstrating a decrease in unit-cell volume. The intensities of the diffraction peaks were decreased simultaneously, suggesting that the distance between adjacent molecules is shorter during the pressurization, which is in agreement with the observations made concerning the emission spectra and Raman spectra. The XRD patterns beyond 3.8 GPa became blurry, hinting at the emergence of an amorphous phase, which is associated with the emission decrease at higher pressure. The molecular arrangement at this point was not as regular as in the initial state, which indicates that the system progressively evolved into a disordered state. As a result, the degree of crystallinity was reduced continuously, eventually leading to the amorphous state at 10.1 GPa, consistent with the results from WXRD measurements (Figure S9 in the Supporting Information). No new diffraction peaks were observed, suggesting that the phase transition did not occur during the whole process. Moreover, the ADXRD pattern returned to the initial state after the pressure was released to ambient pressure, demonstrating that the original molecular arrangement of M2 was restored. All these features make M2 a good candidate as visible colorimetric pressure sensor by applying a design strategy of single-direction extension of the molecular structure.

In summary, two new organic dyes, M1 and M2, containing flexible TPE and rigid PI units were designed and synthesized. They showed observable fluorescent signals during pressure measurements within a range of 0.0–10.1 GPa, and presented a one-dimensional linear relationship between the applied pressure and the maximum emission-peak wavelengths with good reversibility. M2 displayed a higher piezochromic contrast (102 nm) and better sensitivity (11.19 nm GPa^{-1}) than M1 (69 and 6.12 nm GPa^{-1}) owing to the increased long-to-short axis ratio that resulted from the introduction of one more phenyl ring between the TPE and PI units. The in situ UV/Vis absorption spectra indicated a flattening of phenyl rings in the TPE unit. The intermolecular interactions were enhanced and no phase transition was involved in the pressurizing–depressurizing process as evidenced by in situ Raman spectroscopy. The ADXRD patterns with high-intensity synchrotron radiation showed that M2 maintained the original molecular structure under a high pressure of 10.1 GPa. The results illustrate that there exists a supra-amplification effect influencing the ability to respond to high external pressure, and that piezochromic contrast and reversibility can be tuned by simultaneously adjusting the molecular structure in high-pressure experiments. Results from our experiments not only deepen the understanding of piezochromism, but also help to develop a more comprehensive general strategy to evaluate high-pressure-responsive performances. Compounds with further-extended molecular structure are under investigation and the results will be reported in the near future.

Experimental Section

1-Phenyl-2-(4-(1,2,2-triphenylvinyl)phenyl)-1*H*-phenanthro[9,10-*d*]imidazole (M1)

(2-Bromoethene-1,1,2-triyl)tribenzene (0.50 g, 1.00 mmol), 1-phenyl-2-(4-(4,4,5,5-tetramethyl-1,3,2-dioxaborolan-2-yl)phenyl)-1*H*-phenanthro[9,10-*d*]imidazole (0.37 g, 1.10 mmol), K_2CO_3 (0.28 g, 2.00 mmol), and tetrakis(triphenylphosphine)palladium(0) (11.60 mg, 0.01 mmol) were added to a round-bottomed flask equipped with a reflux condenser, and dissolved in methylbenzene (6.00 mL) and H_2O (1.00 mL). The reaction mixture was heated at 85 °C for 24 h, quenched with water, and extracted with chloroform. The combined organic phases were dried over $MgSO_4$ and concentrated under reduced pressure. After solvent evaporation, the liquid was purified by column chromatography using petroleum ether/methylene chloride as the eluent to afford a white solid (0.63 g). Yield: 50.20 %. ^{1}H NMR (500 MHz, DMSO): $\delta=8.93$ (d, $J=8.51$ Hz, 1H), 8.88 (d, $J=8.5$ Hz, 1H), 8.67 (d, $J=7.84$ Hz, 1H), 7.78 (t, $J=7.22$ Hz, 7.10 Hz, 1H), 7.71–7.64 (m, 6H), 7.57 (t, $J=7.17$ Hz, 7.07 Hz, 1H), 7.35–7.32 (m, 3H), 7.18–7.06 (m, 10H), 6.99–6.92 ppm (m, 8H); ^{13}C NMR (500 MHz, $CDCl_3$): $\delta=143.43$, 131.30, 129.08, 128.72, 127.74, 127.67, 126.59, 123.09, 120.87, 77.28, 77.03, 76.78 ppm; FTIR (KBr): $\tilde{\nu}=3116$, 3067, 3045, 3033, 2977, 2882, 2373, 2063, 1910, 1779, 1632, 1333, 1271, 1184, 1088, 1024, 960, 862, 794, 737, 645, 598, 524, 464, 399 cm^{-1}; MALDI-TOF-MS: *m/z* calcd for $C_{47}H_{32}N_2$: 624.77; found: 624.45; elemental analysis calcd (%) for $C_{47}H_{32}N_2$: C 90.35, H 5.16, N 4.48; found: C 90.13, H 5.14, N 4.24.

1-Phenyl-2-(4′-(1,2,2-triphenylvinyl)-[1,1′-biphenyl]-4-yl)-1*H*-phenanthro[9,10-*d*]imidazole (M2)

(2-(4-Bromophenyl)ethene-1,1,2-triyl)tribenzene (1.00 g, 2.43 mmol), 1-phenyl-2-(4-(4,4,5,5-tetramethyl-1,3,2-dioxaborolan-2-yl)phenyl)-1*H*-phenanthro[9,10-*d*]imidazole (1.39 g, 2.80 mmol), K_2CO_3 (0.69 g, 5.00 mmol), and tetrakis(triphenylphosphine)palladium(0) (28.07 mg, 0.02 mmol) were added to a round-bottomed flask equipped with a reflux condenser, and dissolved in methylbenzene (17.50 mL) and H_2O (3.00 mL). The reaction mixture was heated at 85 °C for 24 h, quenched with water, and extracted with chloroform. The combined organic phases were dried over $MgSO_4$ and concentrated under reduced pressure. After solvent evaporation, the liquid was purified by column chromatography using petroleum ether/methylene chloride as the eluent to afford a white

solid (1.21 g). Yield: 62.15%. ^{1}H NMR (500 MHz, DMSO): δ = 8.95 (d, J = 8.43 Hz, 1H), 8.90 (d, J = 8.58 Hz, 1H), 8.72 (d, J = 6.73 Hz, 1H), 7.81–7.69 (m, 7H), 7.64 (s, 4H), 7.59 (t, J = 8.18 Hz, 8.3 Hz, 1H), 7.53 (d, J = 8.41 Hz, 2H), 7.37 (t, J = 8.12 Hz, 7.22 Hz, 1H), 7.19–7.09 (m, 10H), 7.06–6.99 ppm (m, 8H); ^{13}C NMR (500 MHz, $CDCl_3$): δ = 131.87, 131.42, 131.34, 127.72, 126.13, 123.12, 120.91, 77.28, 77.03, 76.78 ppm; FTIR (KBr): $\tilde{\nu}$ = 3117, 3039, 2975, 2878, 2004, 1929, 1854, 1778, 1710, 1583, 1447, 1392, 1305, 1219, 1054, 989, 852, 746, 677, 620, 567, 471, 399 cm^{-1}; MALDI-TOF-MS: m/z calcd for $C_{53}H_{36}N_2$: 700.87; found: 700.16; elemental analysis calcd (%) for $C_{53}H_{36}N_2$: C 90.83, H 5.18, N 4.00; found: C 90.57, H 5.10, N 4.28.

CCDC 1052087 contains the supplementary crystallographic data for this paper. These data are provided free of charge by The Cambridge Crystallographic Data Centre.

Acknowledgements

This research is supported by the Ministry of Science and Technology of China (2013CB834801, 2016YFB0401001), the National Science Foundation of China (21374038), and the Jilin Provincial Science and Technology Department (20160101302JC).

Keywords: phenanthrene[9,10-*d*]imidazole · piezochromic sensitivity · quantum efficiency · tetraphenylethylene · X-ray diffraction

[1] a) Y. Sagara, T. Kato, *Nat. Chem.* **2009**, *1*, 605–610; b) Z. Chi, X. Zhang, B. Xu, X. Zhou, C. Ma, Y. Zhang, S. Liu, J. Xu, *Chem. Soc. Rev.* **2012**, *41*, 3878–3896; c) P. Schattling, F. D. Jochuma, P. Theato, *Polym. Chem.* **2014**, *5*, 25–36.

[2] a) H. Li, X. Zhang, Z. Chi, B. Xu, W. Zhou, S. Liu, Y. Zhang, J. Xu, *Org. Lett.* **2011**, *13*, 556–559; b) T. Han, Y. Zhang, X. Feng, Z. Lin, B. Tong, J. Shi, J. Zhi, Y. Dong, *Chem. Commun.* **2013**, *49*, 7049–7051; c) Z. V. Todres, *J. Chem. Res.* **2004**, *2004*, 89–93; d) Z. Ma, Z. Wang, M. Teng, Z. Xu, X. Jia, *ChemPhysChem* **2015**, *16*, 1811–1828.

[3] a) P. F. McMillan, *Chem. Soc. Rev.* **2006**, *35*, 855–857; b) Z. Mao, Z. Yang, Y. Mu, Y. Zhang, Y. Wang, Z. Chi, C. Lo, S. Liu, A. Lien, J. Xu, *Angew. Chem. Int. Ed.* **2015**, *54*, 6270–6273; *Angew. Chem.* **2015**, *127*, 6368–6371.

[4] a) P. Pritchard, *Fox and McDonald's Introduction to Fluid Mechanics*, 8th ed., Wiley, Hoboken, **2012**, pp. 76–83; b) D. Crane, *Dictionary of Aeronautical Terms*, Aviation Supplies & Academics, Newcastle, **1997**, pp. 194–206.

[5] a) M. S. Kwon, J. Gierschner, S. Yoon, S. Y. Park, *Adv. Mater.* **2012**, *24*, 5487–5492; b) A. Pucci, F. Di Cuia, F. Signori, G. Ruggeri, *J. Mater. Chem.* **2007**, *17*, 783–790; c) B. R. Crenshaw, M. Burnworth, D. Khariwala, A. Hiltner, P. T. Mather, R. Simha, C. Weder, *Macromolecules* **2007**, *40*, 2400–2408.

[6] K. Nagura, S. Saito, H. Yusa, H. Yamawaki, H. Fujihisa, H. Sato, Y. Shimoikeda, S. Yamaguchi, *J. Am. Chem. Soc.* **2013**, *135*, 10322–10325.

[7] a) Y. Wang, X. Tan, Y. M. Zhang, S. Zhu, I. Zhang, B. Yu, K. Wang, B. Yang, M. Li, B. Zou, S. X. Zhang, *J. Am. Chem. Soc.* **2015**, *137*, 931–939; b) Y. Wang, I. Zhang, B. Yu, X. Fang, X. Su, Y. Zhang, T. Zhang, B. Yang, M. Li, S. X. Zhang, *J. Mater. Chem. C* **2015**, *3*, 12328–12334; c) Q. Qi, J. Qian, X. Tan, J. Zhang, L. Wang, B. Xu, B. Zou, W. Tian, *Adv. Funct. Mater.* **2015**, *25*, 4005–4010.

[8] a) L. Wang, K. Wang, B. Zou, K. Ye, H. Zhang, Y. Wang, *Adv. Mater.* **2015**, *27*, 2918–2922; b) Z. Zhang, D. Yao, T. Zhou, H. Zhang, Y. Wang, *Chem. Commun.* **2011**, *47*, 7782–7784.

[9] a) Y. Dong, B. Xu, J. Zhang, X. Tan, L. Wang, J. Chen, H. Lv, S. Wen, B. Li, L. Ye, B. Zou, W. Tian, *Angew. Chem. Int. Ed.* **2012**, *51*, 10782–10785; *Angew. Chem.* **2012**, *124*, 10940–10943; b) C. Dou, D. Chen, J. Iqbal, Y. Yuan, H. Zhang, Y. Wang, *Langmuir* **2011**, *27*, 6323–6329; c) Y. Sagara, T. Mutai, I. Yoshikawa, K. Araki, *J. Am. Chem. Soc.* **2007**, *129*, 1520–1521.

[10] a) B. Xu, Z. Chi, X. Zhang, H. Li, C. Chen, S. Liu, Y. Zhang, J. Xu, *Chem. Commun.* **2011**, *47*, 11080–11082; b) A. L. Balch, *Angew. Chem. Int. Ed.* **2009**, *48*, 2641–2644; *Angew. Chem.* **2009**, *121*, 2679–2682.

[11] a) D. A. Davis, A. Hamilton, J. Yang, L. D. Cremar, D. V. Gough, S. L. Potisek, M. T. Ong, P. V. Braun, T. J. Martınez, S. R. White, J. S. Moore, N. R. Sottos, *Nature* **2009**, *459*, 68–72; b) C. M. Martin, S. Guha, M. Chandrasekhar, H. R. Chandrasekhar, R. Guentner, P. Scanduicci de Freitas, U. Scherf, *Phys. Rev. B* **2003**, *68*, 115203; c) M. Knaapila, Z. Konôpková, M. Torkkeli, D. Haase, H.-P. Liermann, S. Guha, U. Scherf, *Phys. Rev. E* **2013**, *87*, 022602; d) M. Knaapila, R. Stepanyan, D. Haase, S. Carlson, M. Torkkeli, Y. Cerenius, U. Scherf, S. Guha, *Phys. Rev. E* **2010**, *82*, 051853; e) M. Knaapila, M. Torkkeli, Z. Konôpková, D. Haase, H. Liermann, U. Scherf, S. Guha, *Macromolecules* **2013**, *46*, 8284–8288.

[12] Y. Wang, X. Lü, W. Yang, T. Wen, L. Yang, X. Ren, L. Wang, Z. Lin, Y. Zhao, *J. Am. Chem. Soc.* **2015**, *137*, 11144–11149.

[13] a) L. He, F. Xiong, S. Li, Q. Gan, G. Zhang, Y. Li, B. Zhang, B. Chen, G. Yang, *J. Phys. Chem. B* **2004**, *108*, 7092–7097; b) L. He, H. Li, J. Fan, S. Li, Q. Gan, G. Zhang, B. Zhang, Y. Li, G. Yang, *Chem. Phys. Lett.* **2003**, *378*, 263–268.

[14] a) R. Misra, T. Jadhav, B. Dhokale, S. M. Mobin, *Chem. Commun.* **2014**, *50*, 9076–9078; b) C. Li, X. Luo, W. Zhao, Z. Huang, Z. Liu, B. Tong, Y. Dong, *Sci. China Chem.* **2013**, *56*, 1173–1177; c) J. Q. Shi, W. J. Zhao, C. H. Li, Z. P. Liu, Z. S. Bo, Y. P. Dong, Y. Q. Dong, B. Z. Tang, *Chin. Sci. Bull.* **2013**, *58*, 2723–2727.

[15] a) X. Luo, J. Li, C. Li, L. Heng, Y. Q. Dong, Z. Liu, Z. Bo, B. Z. Tang, *Adv. Mater.* **2011**, *23*, 3261–3265; b) S. Xu, T. Liu, Y. Mu, Y. Wang, Z. Chi, C. Lo, S. Liu, Y. Zhang, A. Lien, J. Xu, *Angew. Chem. Int. Ed.* **2015**, *54*, 874–878; *Angew. Chem.* **2015**, *127*, 888–892.

[16] a) C. Y. K. Chan, Z. Zhao, J. W. Y. Lam, J. Liu, S. Chen, P. Lu, F. Mahtab, X. Chen, H. H. Y. Sung, H. S. Kwok, Y. Ma, I. D. Williams, K. S. Wong, B. Z. Tang, *Adv. Funct. Mater.* **2012**, *22*, 378–389; b) J. Y. Kim, T. Yasuda, Y. S. Yang, C. Adachi, *Adv. Mater.* **2013**, *25*, 2666–2671.

[17] a) J. Wang, J. Mei, R. Hu, J. Z. Sun, A. Qin, B. Z. Tang, *J. Am. Chem. Soc.* **2012**, *134*, 9956–9966; b) W. Z. Yuan, Y. Tan, Y. Gong, P. Lu, J. W. Lam, X. Y. Shen, C. Feng, H. H. Sung, Y. Lu, I. D. Williams, J. Z. Sun, Y. Zhang, B. Z. Tang, *Adv. Mater.* **2013**, *25*, 2837–2843.

[18] a) X. Zhou, H. Y. Li, Z. G. Chi, B. J. Xu, X. Q. Zhang, Y. Zhang, S. W. Liu, J. R. Xu, *J. Fluoresc.* **2012**, *22*, 565–572; b) Z. Zhao, J. W. Y. Lam, B. Z. Tang, *J. Mater. Chem.* **2012**, *22*, 23726–23740.

[19] a) C. Wang, B. Xu, M. Li, Z. Chi, Y. Xie, Q. Li, Z. Li, *Mater. Horiz.* **2016**, *3*, 220–225; b) C. Dou, L. Han, S. Zhao, H. Zhang, Y. Wang, *J. Phys. Chem. Lett.* **2011**, *2*, 666–670.

[20] Y. Q. Dong, J. W. Y. Lam, B. Z. Tang, *J. Phys. Chem. Lett.* **2015**, *6*, 3429–3436.

[21] H. H. Chou, Y. H. Chen, H. P. Hsu, W. H. Chang, Y. H. Chen, C. H. Cheng, *Adv. Mater.* **2012**, *24*, 5867–5871.

[22] a) Z. Gao, G. Cheng, F. Shen, S. Zhang, Y. Zhang, P. Lu, Y. Ma, *Laser Photonics Rev.* **2014**, *8*, L6–L10; b) Z. Wang, P. Lu, S. Chen, Z. Gao, F. Shen, W. Zhang, Y. Xu, H. S. Kwok, Y. Ma, *J. Mater. Chem.* **2011**, *21*, 5451–5456.

[23] a) Y. Zhang, S. L. Lai, Q. X. Tong, M. F. Lo, T. W. Ng, M. Y. Chan, Z. C. Wen, J. He, K. S. Jeff, X. L. Tang, W. M. Liu, C. C. Ko, P. F. Wang, C. S. Lee, *Chem. Mater.* **2012**, *24*, 61–70; b) W. C. Chen, Y. Yuan, G. F. Wu, H. X. Wei, L. Tang, Q. X. Tong, F. L. Wong, C. S. Lee, *Adv. Opt. Mater.* **2014**, *2*, 626–631.

[24] a) H. Huang, Y. Wang, S. Zhuang, X. Yang, L. Wang, C. Yang, *J. Phys. Chem. C* **2012**, *116*, 19458–19466; b) K. Wang, F. Zhao, C. Wang, S. Chen, D. Chen, H. Zhang, Y. Liu, D. Ma, Y. Wang, *Adv. Funct. Mater.* **2013**, *23*, 2672–2680.

[25] N. Miyaura, A. Suzuki, *Chem. Commun.* **1979**, 866–867.

[26] a) C. Feng, K. Wang, Y. Xu, L. Liu, B. Zou, P. Lu, *Chem. Commun.* **2016**, *52*, 3836–3839; b) Y. Zhang, K. Wang, G. Zhuang, Z. Xie, C. Zhang, F. Cao, G. Pan, H. Chen, B. Zou, Y. Ma, *Chem. Eur. J.* **2015**, *21*, 2474–2479.

[27] S. Y. Li, Q. Wang, Y. Qian, S. Q. Wang, Y. Li, G. Q. Yang, *J. Phys. Chem. A* **2007**, *111*, 11793–11800.

Manuscript received: October 21, 2016

Accepted Article published: October 30, 2016

Final Article published: ■■ ▮▮, 0000

COMMUNICATION

Piezochromic Effects

Z. Gao, K. Wang, F. Liu, C. Feng, X. He, J. Li, B. Yang, B. Zou, P. Lu**

■■ – ■■

Enhanced Sensitivity and Piezochromic Contrast through Single-Direction Extension of Molecular Structure

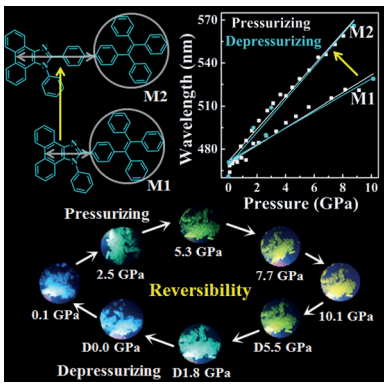

Light them up: Two piezochromic materials containing phenanthro[9,10-*d*]imidazole and tetraphenylethylene (M1 and M2) are developed. Based on the linear relationship between the applied pressure and the emission-peak wavelengths in both pressurizing and depressurizing cycles, quantitative sensitivity for piezochromism is denoted accordingly. M2 displays better piezochromic contrast and sensitivity than M1, originating from the longer long-to-short axis ratio of M2.